Δελτίο της Ελληνικής Γεωλογικής Εταιρίας, τόμος L, σελ. 334-344
Πρακτικά 14ου Διεθνούς Συνεδρίου, Θεσσαλονίκη, Μάιος 2016

Bulletin of the Geological Society of Greece, vol. L, p. 334-344
Proceedings of the 14th International Congress, Thessaloniki, May 2016

GEOMORPHOLOGY, SEDIMENTOLOGY AND GEOCHEMISTRY IN THE MARINE AREA BETWEEN SIFNOS AND KIMOLOS ISLANDS, GREECE

Karageorgis A.P.[1], Ioakim Chr.[2], Rousakis G.[1], Sakellariou D.[1], Vougioukalakis G.[2], Panagiotopoulos I.P.[1], Zimianitis E.[2], Koutsopoulou E.[2], Kanellopoulos Th.[1], Papatrechas Ch.[2], Georgiou P.[1], Xirokostas N.[2], Stavrakaki I.[1], Vakalas I.[2], Morfis I.[1], Koutsovitis P.[2], Drakopoulou P.[1], Kyriakidou Ch.[1] and Marantos I.[2]

[1]Hellenic Centre for Marine Research, 46.7 km Athens-Sounio Ave., 19013 Anavyssos, Greece, ak@hcmr.gr, rousakis@hcmr.gr, sakell@hcmr.gr, jpanagiot@hcmr.gr, thkan@hcmr.gr, pgeorg@hcmr.gr, istavrakaki@hcmr.gr, gianmor@hcmr.gr, vivi@hcmr.gr, hkyriakid@hcmr.gr

[2]Institute of Geology and Mineral Exploration, 1st Spirou Louis St., Olympic Village, 13677, Acharnae, Greece, ioakim@igme.gr, gvoug@igme.gr, zimianitis@igme.gr, ekoutsop@upatras.gr, papatrechas@windowslive.com, xirikostas@igme.gr, vakalas@upatras.gr, petroskoutsovitis@yahoo.com, marantos@igme.gr

Abstract

An extensive oceanographic survey was conducted in the marine area between Kimolos and Sifnos Islands, a rather poorly-studied sector of the Aegean Sea, in order to gain better understanding of submarine geomorphological features and associated sediment provenance. Multi-beam bathymetry and surface sediment sampling with a box corer were carried out on board R/V Aegaeo, followed by grain-size analysis, XRD and XRF measurements. A large circular depression was identified north of Kimolos reaching a water depth of 743 m, filled with fine-grained sediments. Surface sediment distribution is characterized by gradual decrease in grain-size from silty sand to silt in a S-N direction. The mineralogical composition comprises calcite, Mg-calcite, aragonite, dolomite, quartz, K-feldspars, plagioclase, amphiboles and clay minerals. Major sediment provinces identified were: (i) the shallow sector proximal to Kimolos, characterized by higher contents in Si, Al, K, Rb and Ba; (ii) the deep area west of Sifnos, including the large depression, characterized by higher contents in Fe, Ti, Na, Mg, S, Cr, Cu, Ni, V, Zn; and (iii) the south passage between Kimolos and Sifnos, which exhibits higher Ca, S, and Sr contents. Manganese enrichment was observed in and around the bathymetric depression, where Mn oxides act efficiently as scavengers of a suite of metals.

Keywords: *sediment provenance, depression, carbonate minerals, manganese oxides.*

Περίληψη

Στην ελάχιστα μελετημένη θαλάσσια περιοχή μεταξύ των νησιών Σίφνου και Κιμώλου πραγματοποιήθηκε μια εκτεταμένη ωκεανογραφική μελέτη, με σκοπό την καταγραφή της υποθαλάσσιας μορφολογίας και των χαρακτηριστικών των επιφανειακών ιζημάτων, καθώς και της πηγής προέλευσης αυτών. Έγιναν καταγραφές με πολυδεσμικό βυθόμετρο και δειγματοληψίες επιφανειακών ιζημάτων με box corer με το Ω/Κ Αιγαίο

και ακολούθησαν αναλύσεις μεγέθους κόκκων, ορυκτολογίας και γεωχημείας. Ένα μεγάλο βαθυμετρικό βύθισμα εντοπίστηκε βόρεια της Κιμώλου, με μέγιστο βάθος 743 μ., που συγκεντρώνει λεπτόκοκκα ιζήματα. Η κατανομή των ιζημάτων ως προς το μέγεθος κόκκων χαρακτηρίζεται από σταδιακή μείωση του μεγέθους από νότο προς βορρά. Η ορυκτολογική σύσταση περιλαμβάνει ασβεστίτη, Mg-ασβεστίτη, αραγωνίτη, δολομίτη, χαλαζία, Κ-άστριους, πλαγιόκλαστα, αμφίβολους και αργιλικά ορυκτά. Οι κύριες ιζηματολογικές επαρχίες που αναγνωρίστηκαν είναι 1) η ρηχή περιοχή πλησίον της Κιμώλου, με υψηλό περιεχόμενο σε Si, Al, K, Rb και Ba, 2) η βαθιά περιοχή δυτικά της Σίφνου, όπου εμφανίζεται και το μεγάλο βύθισμα, που χαρακτηρίζεται από υψηλό περιεχόμενο σε Fe, Ti, Na, Mg, S, Cr, Cu, Ni, V, Zn και 3) το στενό μεταξύ Σίφνου και Κιμώλου, με υψηλότερο περιεχόμενο σε Ca, S και Sr. Στο βύθισμα αυτό, παρατηρήθηκε σημαντικός εμπλουτισμός των ιζημάτων σε μαγγάνιο, ενώ τα οξείδια του Mn φαίνεται να προσροφούν διάφορα μέταλλα.
Λέξεις κλειδιά: *προέλευση ιζημάτων, ανθρακικά ορυκτά, οξείδια του μαγγανίου.*

1. Introduction

The South Aegean Volcanic Arc is the major geomorphological feature of the entire Aegean Sea, featuring a series of volcanoes as Methana and Milos to the west, and Santorini and Nisyros to the east. Milos and Kimolos islands lie in the westernmost sector the Cyclades Plateau, whereas Sifnos Island lies further to the NE, on a broad shelf characterized generally by water depths <400 m (Poulos, 2009). The marine area between the latter islands has been investigated by Piper and Perissoratis (2003) in respect to the sedimentary and tectonic Quaternary evolution, however, the sedimentological features of the area, as well as associated depositional processes of the sediments, are largely unknown.

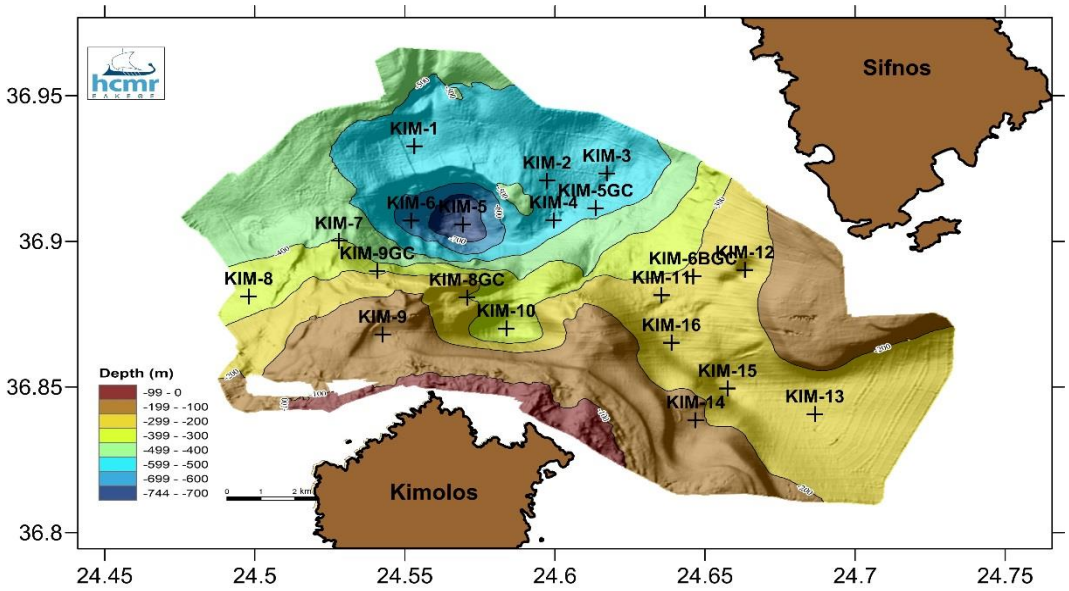

Figure 1 - Sampling stations location superimposed on swath bathymetry map.

The Hellenic Centre for Marine Research (HCMR) and the Institute of Geology and Mineral Explorations (IGME) have been conducting since 2013 a multifaceted oceanographic project in the Aegean Sea named 'Aegean Explorations/YPOTHER'. As part of this project, a cruise (AEX-2) was organized in 2014 in SW Cyclades with initial aim to investigate a prominent submarine depression located between Kimolos and Sifnos; data collected earlier by the Hellenic Hydrographic Service

and IGME had recorded a semi-circular submarine feature with water depths up to 720 m, some 200 m deeper than the surrounding seafloor.

Multi-beam bathymetry, seismic profiling, and remotely operated vehicle dives were utilized to provide information on this peculiar geomorphological feature, whereas surface sediments and gravity cores were collected to better understand the geochemical characteristics of the area. Here we present preliminary results on the submarine geomorphology and associated surface sediment properties, documented for the first time. Sediment transport and depositional processes are discussed, whilst sediment provenance is considered in respect to differing island lithology.

2. Materials and methods

The oceanographic cruise AEX-2 was carried out between 30 April and 9 May 2014 on board R/V Aegaeo. The bathymetry survey (total length of 250 nm) was performed with a hull-mounted SeaBeam 2120 multi-beam echo sounder (frequency of operation: 20 kHz; applied half-swath angle: 58-60°; maximum received beams: 117-121; swath overlapping: a minimum of 30%; across-track resolution: <14 m; along-track resolution: <10 m). Several sound velocity profiles, obtained from conductivity-temperature vs depth (CTD) casts at deep sites (600-630 m) in the study area, were incorporated into the acquisition software of the multi-beam system to calibrate the position and accuracy of recorded depth values. The estimated error in the vertical and horizontal dimension was within 0.5% and 10 m, respectively.

Sixteen surface sediments (0-2 cm) were collected by means of a stainless-steel box corer. In addition, 4 gravity core tops (0-3 cm) were used for geochemical analysis only, due to limited sample quantity. Grain-size measurements were performed with the pipette method, after separation of the >63 μm fraction by wet sieving, and textural sediment classification followed the subdivisions of Folk (1974) (Table 1). The samples were analyzed for the determination of their mineralogical composition using X-Ray diffraction (XRD). The X-Ray diffractometer was a Panalytical X'pert-Pro with a Cu X-ray tube (K_α of Cu, $\lambda = 1.5405$ Å), graphite monochromator, an applied voltage 30 kV and a 40 mA current. The random powder mounts of samples, prepared by back loading, were scanned from 2-70º 2θ. Data were evaluated with the XPert High-Score (Version 2004) (Panalytical B.V., Almelo, The Netherlands) and the EVA® software (DIFFRACplus EVA v12.0, Bruker AXS GmbH) and managed with the PDF-2 database (International Centre for Diffraction Data, Newtown Square, PA, USA). The clay fraction (<2 μm) was separated by settling and oriented glass slides were prepared for the determination of clay minerals. X-Ray diffraction analysis was performed from 2-35° 2θ (i) from air-dried samples, (ii) after ethylene glycol solvation at 60 °C to ensure maximum saturation and (iii) after heating at 490 °C. The mineral phases were quantified with a standardless Rietveld refinement routine using TOPAS® software, and the quantification errors were less than 1% (Table 2). Polished thin sections were prepared and examined in the SEM laboratory of IGME, (JEOL JSM-5600 coupled with an Oxford Instruments EDS system), whereas the analysis conditions were 30 keV acceleration voltage, 3 nA beam current and a spot diameter of 10-30 μm.

Bulk samples were oven dried, ground to a fine powder in a Fritsch motorized mill with agate mortar and balls and were analyzed for their chemical composition in a Panalytical PW-2400 wavelength X-Ray fluorescence analyzer, equipped with Rh-tube. Major elements were determined in fused beads and minor elements in pressed-powder pellets following the procedure of Karageorgis *et al.* (2005, 2009). Part of the same samples were pulverized to <200 mesh in an agate mill, was digested with a mixture of HCl-HNO_3-HF acids and were analyzed for a series of trace elements by Inductively Coupled Plasma-Atomic Emission Spectroscopy (ICP-MS). Loss on ignition (LOI) was determined by estimating the weight loss after burning 1 g of sample for 1 h at 1000°C. The geochemical data set comprised also the top (0-4 cm) sediment of four gravity cores (Table 1).

Table 1 - Grain-size classes and major/minor elemental contents for surface sediments from Kimolos-Sifnos marine area.

Station	depth	sand	silt	clay	SiO_2	Al_2O_3	Fe_2O_3	TiO_2	K_2O	Na_2O	CaO	MgO	SO_3	P_2O_5	MnO	LOI	Sum	As	Ba	Co	Cr	Cu	Mn	Ni	Pb	Rb	Sr	V	Zn
	m	%																$\mu g\ g^{-1}$											
KIM-1	547	1.7	94.2	4.1	25.7	7.2	2.99	0.330	1.49	2.85	24.6	3.30	0.702	0.119	0.273	31.5	101.1	17	340	17	94	37	2700	72	41	62	884	67	88
KIM-2	518	4.0	92.0	4.0	26.1	7.1	2.89	0.324	1.49	2.86	24.7	3.19	0.683	0.112	0.210	31.4	101.0	20	374	19	88	34	2145	71	42	61	883	66	89
KIM-3	575	6.1	88.4	5.5	25.9	7.3	2.95	0.326	1.49	3.16	24.0	3.23	0.775	0.118	0.242	31.6	101.2	17	372	17	84	37	2365	71	43	61	878	65	93
KIM-4	518	4.2	90.6	5.2	25.6	7.1	2.91	0.325	1.48	2.94	24.6	3.24	0.712	0.114	0.189	31.1	100.3	20	363	18	82	34	1828	69	43	61	877	63	90
KIM-5	735	5.4	87.2	7.4	24.2	6.9	3.00	0.312	1.43	3.56	23.8	3.29	0.786	0.127	0.576	32.9	100.9	23	340	24	89	36	5833	79	43	59	853	65	93
KIM-6	639	14.4	80.9	4.7	22.1	7.1	2.69	0.291	1.21	2.67	26.8	3.46	0.671	0.118	0.169	33.5	100.8	18	302	17	82	36	1722	68	40	55	896	63	85
KIM-7	383	44.2	53.7	2.1	20.8	5.4	2.07	0.233	1.09	1.87	30.7	3.37	0.575	0.099	0.097	33.0	99.3	17	340	11	57	22	1016	43	31	45	934	50	66
KIM-8	332	35.3	62.4	2.3	26.2	6.3	2.35	0.280	1.37	2.17	27.2	3.03	0.566	0.106	0.143	30.5	100.3	19	458	10	59	24	1296	45	37	53	914	52	80
KIM-9	173	53.2	44.7	2.1	27.3	8.0	2.50	0.229	1.32	2.14	24.7	2.47	0.566	0.081	0.110	30.0	99.4	17	672	11	40	18	1252	29	33	60	1347	44	74
KIM-10	367	40.0	57.6	2.4	32.4	7.5	2.65	0.314	1.65	2.45	23.5	2.37	0.610	0.103	0.113	26.4	100.1	19	631	12	58	24	1140	43	37	64	963	57	83
KIM-11	274	41.4	56.9	1.7	25.0	5.9	2.27	0.272	1.27	2.02	28.4	2.99	0.664	0.101	0.093	30.8	99.8	17	395	10	60	22	965	42	29	50	1014	49	63
KIM-12	245	62.5	36.2	1.4	23.9	5.2	2.49	0.250	1.11	1.92	30.1	2.75	0.589	0.093	0.083	31.0	99.4	10	323	11	59	19	869	40	18	45	1204	46	48
KIM-13	253	41.3	57.4	1.3	24.9	5.6	2.27	0.266	1.22	2.03	28.4	2.94	0.754	0.094	0.097	30.5	99.1	15	371	10	62	23	981	42	23	48	1104	46	55
KIM-14	192	45.3	53.8	0.8	29.6	7.8	2.37	0.263	1.43	2.10	23.9	2.57	0.777	0.085	0.077	28.4	99.3	16	590	9	53	19	821	32	28	60	1139	44	64
KIM-15	280	44.3	53.6	2.1	26.5	5.9	2.49	0.267	1.29	2.07	27.8	2.77	0.697	0.099	0.084	29.9	99.9	15	399	11	62	20	836	41	23	50	1139	47	57
KIM-16	269	39.5	57.6	2.9	26.2	6.0	2.30	0.283	1.32	2.06	27.5	2.93	0.718	0.098	0.098	29.5	99.0	19	414	10	62	23	973	42	26	52	1042	49	61
KIM-5GC	525	-	-	-	26.3	7.2	2.91	0.328	1.48	2.05	26.2	3.16	0.539	0.168	0.232	29.4	100.0	20	330	16	79	33	2182	66	34	59	921	62	77
KIM-6BGC	282	-	-	-	26.2	6.5	2.38	0.299	1.34	1.79	27.3	2.91	0.605	0.101	0.098	30.4	99.9	11	302	8	56	17	473	40	21	45	961	44	44
KIM-8GC	290	-	-	-	31.6	8.7	2.13	0.319	1.63	1.87	23.1	2.54	0.345	0.102	0.103	26.7	99.1	13	437	9	52	18	440	36	51	55	870	46	61
KIM-9GC	316	-	-	-	26.8	6.4	2.49	0.288	1.38	2.73	27.3	3.12	0.502	0.109	0.099	28.5	99.7	18	456	10	56	26	965	41	37	53	972	52	75
mean		30.2	66.7	3.1	26.2	6.75	2.55	0.290	1.37	2.36	26.2	2.98	0.642	0.107	0.159	30.3		17	410	13	67	26	1540	51	34	55	990	54	72
st. dev		20.4	18.9	1.8	2.72	0.92	0.30	0.032	0.15	0.50	2.23	0.32	0.110	0.018	0.115	1.9		3	106	4	15	7	1193	16	9	6	134	9	15

3. Results

3.1. Submarine geomorphology

The seafloor of the survey area north of Kimolos displays a rather complicated relief (Fig. 2). The southern part includes the submarine slopes off Kimolos Island and displays highly irregular morphology with steep slopes, ridges, local highs or mounts and hummocky seafloor close to Kimolos shoreline. This configuration reflects the volcanic origin of the seafloor's substrate of Kimolos volcanic province.

The eastern part of the survey area encompasses the shelf and slope west and south of Sifnos Island. The seafloor displays smooth morphology. A wide shelf extends to the south of Sifnos and passes abruptly to a steep slope facing the northeastern Kimolos shore. The shelf along the western side of Sifnos becomes gradually narrower towards north and passes towards west to a smoothly to moderate steep slope. The morphological characteristics off Sifnos Island reflect the metamorphic origin of the seafloor's substrate.

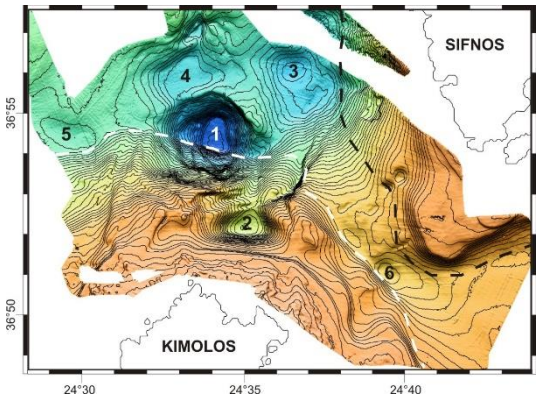

Figure 2 - Numbers 1 to 6: bathymetric depressions. White dashed line: limit of Kimolos volcanic province. Black dashed line: limit of Sifnos metamorphic province. Background: swath bathymetry map.

The northern part of the survey area occupies the southern part of the sedimentary basin which has developed north of Kimolos volcanic province and west of Sifnos metamorphic province. Unlike most flat sedimentary basins, it displays a peculiar relief with local depressions and structural highs spatially alternating. Six noticeable depressions have been labelled with numbers and are shown on the bathymetric map of Fig. 2. Depression Nr. 1 is the deepest and most spectacular among the six, with a maximum depth of 743 m, surrounded by steeply dipping (more than 50%) slopes. It is located at the foot of the northern slope of Kimolos and the dimensions of its floor, at the 730 m depth contour, are 1.6 km in N-S and 1.0 km in E-W direction. The second well-developed depression is Nr. 2, on the northern slope of Kimolos. The dimensions of its floor, at the 360 m depth contour, are 0.9 km and 1.0 km in N-S and E-W direction, respectively, whilst maximum water depth reaches 370 m.

Apart from the depressions Nr. 1 and 2, four more, locally developed, shallower depressions have been mapped. The three of them, i.e. Nrs. 3, 4 and 5, are located in the basin north of Kimolos, whilst depression Nr. 6 marks the narrowest point of the strait between Kimolos volcanic province and Sifnos metamorphic province.

Seismic reflection profiles show that almost all depressions (except depression Nr. 2) are underlain by thick sedimentary deposits of Plio(?)-Quaternary age. Although processing and interpretation of the seismic data is in progress, preliminary results indicate that the formation of the depressions is the result of active tectonic movements and local transtensional deformation and subsidence.

3.2. Sediment grain-size analysis

Surface sediments in the study area are composed of silt and sand, with minor proportions of clay (Fig. 3). Sand percentages up to 53% are observed north of Kimolos, exhibiting a decreasing trend towards the north, whilst the highest sand content (63%) is recorded between Sifnos and Kimolos. Silt is the predominant size class (max. 92%) with relatively higher values observed at the deepest sector of the study area, i.e. the bathymetric depression and its surroundings. In terms of their textural classification, the sediments vary between sandy silt to silt and are illustrated in the ternary diagram of Fig. 3.

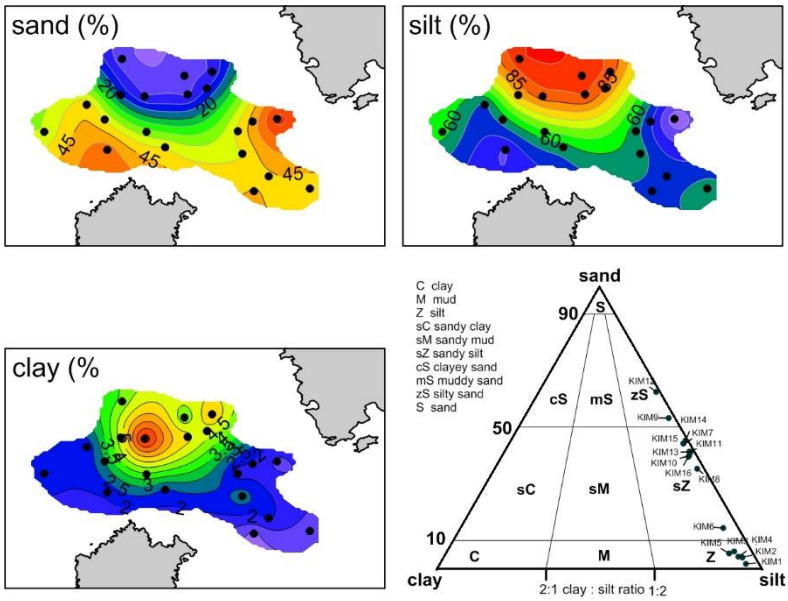

Figure 3 - Spatial distribution of sand, silt and clay percentages. The grain size ternary diagram is also presented (after Folk, 1974).

3.3. Bulk mineralogy and clay minerals

The bulk mineralogical composition comprises carbonate minerals (calcite, Mg-calcite, aragonite and dolomite, from 42.6 to 53.9% in total), quartz (6.4-11.3%), plagioclase (5.4-15.5%) and to a lesser extent K-feldspars and clay minerals (illite, chlorite, kaolinite and traces of smectite) (Table 2). Amphiboles, biotite, barite, pyroxenes, epidote, garnet, magnetite, pyrite, serpentine and talc occur as accessory mineral phases (XRD analysis and SEM observations). Terrigenous minerals comprise quartz, plagioclase, K-feldspars, opal-CT, amphiboles and clay minerals. Calcite peaks at the vicinity of the major bathymetric depression, together with chlorite, illite and partly kaolinite (Fig. 4). Plagioclase, K-feldspars, opal-CT, aragonite, and partly kaolinite and quartz show maxima north of Kimolos, displaying decreasing trends towards the north. Dolomite and hornblende appear to be enriched in the Sifnos-Kimolos strait, and Mg-calcite, shows maxima at the NW and E sectors of the study area (Fig. 4).

Based on detailed optical and SEM microscopy observations, several accessory minerals were identified, as allanite and monazite, which are REE-bearing mineral phases. Allanites have noticeable thorium contents (up to 2.7%), whereas monazites include relatively high amounts of REE and thorium contents (ΣREE + Th=52-60 %). Ti-bearing minerals include ilmenite, Ti-magnetite as well as minor rutile and titanite. In particular, unaltered to slightly altered ilmenite and Ti-magnetite formed hypidiomorphic fine and occasionally medium grained crystals with an estimated modal composition of about 0.5%. Barite is present in all examined sediment samples as well as zircon and zinc/copper oxides.

Table 2 - Mineralogical composition of surface sediments (Cc: calcite, Mg-Cc: magnesium calcite, A: aragonite, D: dolomite, Q: quartz, P: plagioclase, K-F: K-feldspars, Ho: hornblende, O: opal-CT, I: illite, Chl: chlorite, K: kaolinite, Ha: halite).

Sample	Cc	Mg-Cc	A	D	Q	P	K-F	Ho	O	I	Chl	K	Ha
KIM-1	27.6	18.8	2.9	0.9	7.3	6.8	5.3	0.6	2.3	10.9	8.4	4.8	3.4
KIM-2	26.2	19.2	4.0	0.8	7.9	7.4	6.6	0.7	2.1	9.9	8.3	4.8	2.1
KIM-3	26.9	16.4	3.7	0.9	7.1	9.2	6.6	0.8	2.0	10.1	7.9	5.2	3.2
KIM-4	27.3	17.8	3.8	0.7	7.8	7.7	5.8	0.6	1.6	10.6	8.5	4.9	2.9
KIM-5	26.9	19.5	2.9	0.9	6.8	6.1	5.1	0.3	2.0	13.3	8.1	4.2	3.9
KIM-6	27.1	22.6	3.5	0.7	6.4	6.4	5.5	0.6	1.6	11.1	6.3	4.9	3.3
KIM-7	19.6	27.2	5.1	1.5	7.8	8.3	5.6	0.7	2.1	9.5	7.3	3.1	2.2
KIM-8	21.8	19.9	4.6	0.6	8.9	11.2	6.6	0.8	3.7	8.5	6.9	4.4	2.1
KIM-9	22.4	8.9	10.6	0.7	8.8	15.5	8.6	0.6	2.9	10.7	4.8	3.4	2.1
KIM-10	23.5	10.8	7.6	0.7	8.8	11.6	9.6	1.0	4.0	7.9	6.8	5.3	2.4
KIM-11	19.9	21.0	6.0	1.2	9.2	8.9	4.8	1.1	2.5	12.8	7.2	3.2	2.2
KIM-12	24.3	16.9	9.2	2.0	8.9	12.7	2.5	1.1	0.3	11.4	4.8	3.5	2.4
KIM-13	20.9	24.6	7.7	1.1	9.8	5.4	4.5	0.6	2.7	8.9	6.2	4.8	2.8
KIM-14	27.9	8.6	9.6	1.4	11.3	12.8	7.8	1.1	2.6	5.7	5.7	4.6	0.9
KIM-15	25.4	13.6	7.5	1.8	9.4	12.7	5.7	0.7	1.5	8.1	6.8	4.2	2.6
KIM-16	24.0	18.2	5.4	1.3	9.3	12.0	6.9	1.2	1.5	7.1	5.7	4.5	2.9

3.4. Geochemistry of major and minor elements

Calcium is the major elemental component (CaO 23.1-30.7%), followed by Si, Al, Mg and Fe oxides (Table 1). The abundance of biogenic cells and their fragments in the sediments point primarily to a biogenic origin of Ca and Mg, however, plagioclase, detrital calcite and dolomite are also contributors of those elements. Silicon is typical component of aluminosilicate minerals as well as detrital quartz. The mean Si/Al ratio is 3.45, fairly similar to the average shale (3.41; Turekian and Wedepohl, 1961); some higher values (up to 4.1) are observed between Sifnos and Kimolos islands.

Considering the element spatial distribution patterns (Fig. 5), different provinces are identified: i) Si, Al and K contents are more pronounced north of Kimolos, being associated with more coarse-grained, shallow water sediments; ii) Fe, Ti, Na, Mg and partly S exhibit higher contents in the northern sector, which is characterized by finer grain-sizes and deeper waters. It should be noted that Na is mainly related to halite, due to insufficient removal of sea-salt; and iii) Ca is more abundant at the western and eastern sectors of the study area, without indicating any clear association with other major elements.

Minor elements demonstrating the highest mean contents are Mn (1540 μg g^{-1}), Sr (990 μg g^{-1}) and Ba (410 μg g^{-1}). According to their spatial distribution patterns (Fig. 6) the following groups are formed: i) the metals Cr, Cu, Ni, V, Zn and partly Pb exhibit highest contents in the northern sector of the area; ii) Mn, Co and partly As also show maxima in the northern sector but also peak at KIM-5 sampling site, located at the major depression; iii) Ba and Sr decrease in a S-N direction; and iv) Rb shows double maxima at the northern sector and north of Kimolos.

3.5. Factor analysis

In general, variation in sediments' mineralogical and geochemical composition and spatial distribution can be explained by a number of key-factors, i.e. bottom topography and water depth, grain size and other textural characteristics, different provenance, as well as *in situ* biological and geochemical processes.

The complex sedimentological and geochemical features that were identified in the study area were further investigated by multivariate statistics methods, described hereafter, to gain better understanding on the interrelationships of all variables. Exploratory factor analysis (EFA) is a statistical data-reduction method widely applied in geosciences to allow grouping of correlated variables assuming that an underlying causal model exists. Prior to analysis, the data set was checked

for outliers (Box-and-Whisker plots and Grubbs test), checked for normality (Kolmogorov-Smirnov test) and, then, transformed to improve normality and symmetry (Box-Cox transformation and *z*-transformation); a detailed description of the method is given in Karageorgis *et al*. (2009).

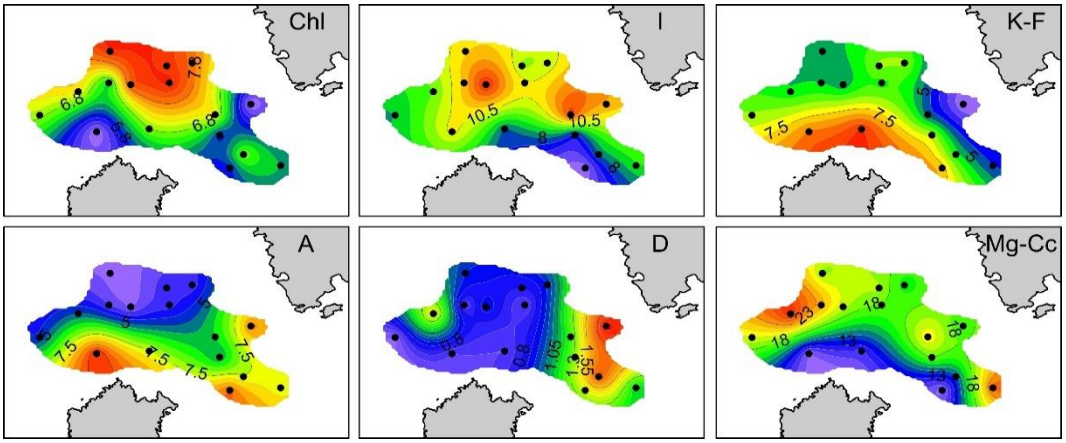

Figure 4 - Spatial distribution of main minerals (%).

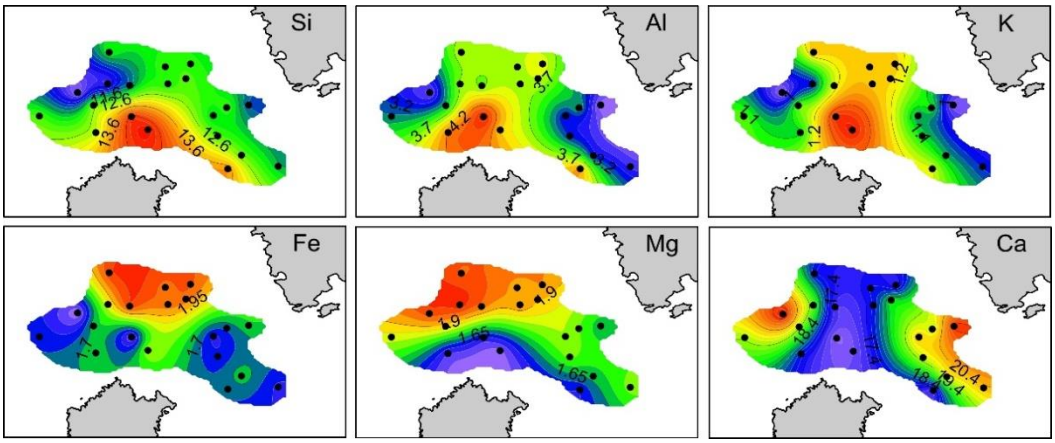

Figure 5 – Spatial distribution of major elements (%).

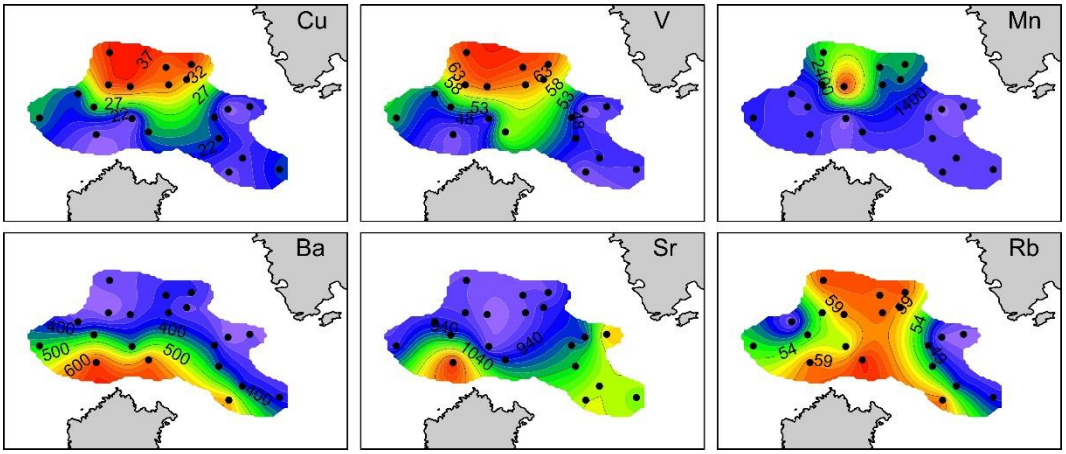

Figure 6 – Spatial distribution of minor elements (μg g^{-1}).

Variables exhibiting low communalities (the squares of correlations) were excluded from EFA and a new model was created. A final 3-factor model solution was selected, which explains 89% of the total variance (Table 3).

Factor 1 (60%) exhibits high loadings for Mn, Fe (and Na), minor elements Co, Cr, Cu, V, Zn, clay content and water depth. Factor 1 may be interpreted as Fe-Mn oxides, amorphous and/or crystalline, which are efficient scavengers of numerous metals (Stumm and Morgan, 1996). Manganese is supplied to the ocean either as Mn-oxide coatings on particulate material delivered by wind/rivers or by deeper sediments through diffusion and early diagenesis (Calvert and Pedersen, 2003). In the north Aegean (Sporades basin), Mn oxides occurred as coatings on fine grained calcite particles or quartz (Karageorgis *et al*., 2005). In the study area, Mn content shows increasing trend towards deeper waters and may be related to lower sedimentation rates, as observed in the Gulf of Lions (Marin and Giresse, 2001). The excess Mn content in the surface sediments is also documented by the Mn/Al ratio, which peaks at the deepest (735 m) KIM-5 sampling site at 1596×10^{-4}, a value several-fold higher than the average shale Mn/Al ratio of 94×10^{-4} (Turekian and Wedepohl, 1961), further suggesting a substantial enrichment of the deeper sediments in Mn oxides and associated minor elements. However, Fe/Al ratio varies between 0.32 and 0.64 (mean 0.51±0.06), which is comparable to the average shale value of 0.59, denoting minor Fe enrichment. Energetically, Mn oxides are much more favourable electron acceptors than iron oxides or sulfate, thus, in the study area, Mn oxides play a primary role on the adsorption and complexation of various metals.

Table 3 - Factor pattern after Varimax rotation.

Variable	F1	F2	F3
Si	-0.286	0.881	-0.238
Al	0.146	0.841	0.024
Fe	0.749	0.275	0.336
Ti	0.297	0.580	0.725
K	0.116	0.955	0.245
Na	0.854	0.266	0.186
Ca	-0.284	-0.902	-0.062
Mg	0.549	-0.440	0.601
Ba	-0.054	0.538	-0.695
Co	0.886	0.024	0.382
Cr	0.629	-0.030	0.695
Cu	0.836	0.025	0.506
Mn	0.947	-0.015	0.190
Ni	0.666	-0.045	0.735
Rb	0.634	0.749	-0.021
Sr	-0.377	-0.274	-0.752
V	0.784	0.167	0.564
Zn	0.864	0.350	0.243
clay	0.714	0.147	0.543
depth	0.628	0.027	0.757

Factor 2 explains 24% of the total variance and exhibits high loadings for Si, Al, K, Rb and moderate loadings for Ti and Ba, thus, representing the group of terrigenous aluminosilicates elements, which are inversely loaded to Ca and Sr, the typical constituents of autochthonous biogenic carbonates. Finally, Factor 3 (5%) with high loadings for Ti, Mg, Cr, Ni and water depth, may be associated

with the presence of minerals such as amphiboles, chlorite, serpentine and talc, derived from the metamorphic rocks of Sifnos Island, whereas Ti-bearing minerals (ilmenite, rutile and titanite) originate in the volcanic, pyroclastic and granitic rocks of Kimolos. The spatial distribution of those elemental ratios to Al (not shown) support this notion.

4. Concluding remarks

Available grain size, quantitative mineralogical and geochemical data provide a unique opportunity to study sediment distribution patterns and provenance, as they exhibit common attributes. The autochthonous biogenic component is very pronounced, illustrated by calcite, Mg-calcite and aragonite, and explains the geochemical behaviour of the elements Ca, Mg and Sr. Calcium in the bulk sediment originates both in the biogenic carbonate minerals but also in the detrital dolomite and plagioclase. For that reason, its spatial distribution does not closely resemble to the distribution patterns of calcite, which is the most abundant mineral. Strontium and aragonite are linearly correlated (R^2=0.871), suggesting that Sr substitutes Ca ions preferentially in aragonite rather than in other carbonate minerals. On the other hand, dolomite clearly originates in the marbles of Sifnos, which are abundant in the island (Matthews and Schliestedt, 1984). Sifnos is also the prime source of chlorite and illite (blue and green schists) and these fine clay minerals settle preferentially into the major bathymetric depression, attracting a variety of chemical elements, which are structural to aluminosilicates and a portion of metals too.

The volcanic formations of Kimolos (Photiadis, 2012) and probably the Kastro and Prassa ignimbrite (Christidis, 2001) are the main sediment contributors in plagioclase, K-feldspars, opal CT, kaolinite and quartz, thus, explaining the distribution patterns of several elements such as Si, Al, K, Ba and Rb. Manganese oxides and hydroxides, associated with most of the metals (Co, Cr, Cu, Ni, V, Zn) due to their high adsorption capacity, appear to be the dominant phase in the northern sector of the study area, including the major depression, but they do not relate to a single mineral phase, most probably due to their amorphous or poorly crystallized nature.

The SE sector of the study area, i.e. the Sifnos-Kimolos strait, is characterized by rather coarse-grained sediments, occurring at depths up to 300 m. On one hand, this is due to the abundance of sand-sized shells and debris of molluscs, but it also implies the presence of strong bottom-currents, which strip out fine-grained sediments. This is in agreement with the early work of Anagnostou *et al.* (1998) as well as the recent observations of Tripsanas *et al.* (2016); the latter authors identified several episodes of intense bottom-current activity during the last 80 ka in the South Aegean Sea, associated with climatic changes.

5. Acknowledgments

We wish to thank the officers and crew of R/V Aegaeo for their invaluable support during field measurements and sampling during the cruise AEX-2. The research cruise was funded by EU/ESPA, YPOTHER project (351008), realized at IGME in collaboration with HCMR.

6. References

Anagnostou, Ch., Richter, D.K., Riedel, D. and Trapp, T., 1998. Recent sediments in the south Cyclades marine area, Aegean Sea, *Bull. Geol. Soc. Greece*, XXXII/2, 193-203.

Calvert, S.E. and Pedersen, T.F., 1993. Geochemistry of recent oxic and anoxic marine sediments: Implications for the geological record, *Mar. Geol.*, 113, 67-88.

Christidis, G.E., 2001. Formation and growth of smectites in bentonites: A case study from Kimolos Island, Aegean, Greece, *Clays and Clay Minerals*, 49(3), 204-215.

Folk, R.L., 1974. *Petrology of sedimentary rocks*, Hemphill, Austin, Texas.

Karageorgis, A.P., Anagnostou, C.L. and Kaberi, H., 2005. Geochemistry and mineralogy of the NW Aegean Sea surface sediments: implications for river runoff and anthropogenic impact, *Appl. Geochem.*, 20(1), 69-88, doi: 10.1016/j.apgeochem.2004.07.008.

Karageorgis, A.P., Katsanevakis, S. and Kaberi, H., 2009. Use of enrichment factors for the assessment of heavy metal contamination in the sediments of Koumoundourou Lake, Greece, *Water Air Soil Poll.*, 204, 243-258, doi: 10.1007/s11270-009-0041-9.

Marin, B. and Giresse, P., 2001. Particulate manganese and iron in recent sediments of the Gulf of Lions continental margin (north-western Mediterranean Sea): deposition and diagenetic process, *Mar. Geol.*, 172, 147-165.

Matthews, A. and Schliestedt, M., 1984. Evolution of the blueschist and greenschist facies rocks of Sifnos, Cyclades, Greece. A stable isotope study of subduction-related metamorphism, *Contrib. Mineral. Petrol.*, 88, 150-163.

Photiadis, A., 2012. Geological map sheet "Kimolos" scale 1:50.000, IGME, 2012.

Piper, D.J.W. and Perissoratis, C., 2003. Quaternary neotectonics of the South Aegean arc. *Mar. Geol.*, 198, 259-288.

Poulos, S.E., 2009. Origin and distribution of the terrigenous component of the unconsolidated surface sediment of the Aegean floor: A synthesis, *Cont. Shelf Res.*, 29, 2045-2060.

Stumm, W. and Morgan, J.J., 1996. *Aquatic Chemistry*, Wiley-Interscience, New York.

Tripsanas, E.K., Panagiotopoulos, I.P., Lykousis, V., Morfis, I., Karageorgis, A.P., Anastasakis, G. and Kontogonis, G., 2016. Late Quaternary bottom-current activity in the South Aegean Sea reflecting climate-driven dense-water production, *Mar. Geol.*, accepted manuscript.

Turekian, K.K. and Wedepohl, K.H., 1961. Distribution of the elements in some major units of the earth's crust, *Bull. Geol. Soc. Am.*, 72, 175-192.